

Article

Not peer-reviewed version

Electro-Optical Properties of Excitons in CdSe Nanoplatelets

[Gerard Zygfryd Czajkowski](#)*

Posted Date: 9 February 2026

doi: 10.20944/preprints202601.2120.v2

Keywords: electroabsorption; nanoplatelets; CdSe; exciton states; Franz-Keldysh effect



Preprints.org is a free multidisciplinary platform providing preprint service that is dedicated to making early versions of research outputs permanently available and citable. Preprints posted at Preprints.org appear in Web of Science, Crossref, Google Scholar, Scilit, Europe PMC.

Copyright: This open access article is published under a [Creative Commons CC BY 4.0 license](#), which permit the free download, distribution, and reuse, provided that the author and preprint are cited in any reuse.

Disclaimer/Publisher's Note: The statements, opinions, and data contained in all publications are solely those of the individual author(s) and contributor(s) and not of MDPI and/or the editor(s). MDPI and/or the editor(s) disclaim responsibility for any injury to people or property resulting from any ideas, methods, instructions, or products referred to in the content.

Article

Electro-Optical Properties of Excitons in CdSe Nanoplatelets

Gerard Zygfryd Czajkowski

Technical University of Bydgoszcz, Aleje Prof. S. Kaliskiego 7, 85-789 Bydgoszcz, Poland; czajk@pbs.edu.pl

Abstract

The constant external electric field, applied to a semiconductor nanostructure with Wannier-Mott excitons, where the electron and the hole interact via central-symmetric Coulomb potential, changes the symmetry of the system. It can be cylindrical symmetry, for the electric field, applied parallel to the z -axis, or a symmetry breaking, for the field parallel to the $x - y$ plane. The symmetry changes affect the optical properties of the system. Below we present a theoretical calculation, obtaining analytical expressions for the optical functions for CdSe Nanoplatelets (reflectivity, transmissivity, absorption coefficient), from which we choose the absorption coefficient, in an external homogeneous electric field. We consider various configurations, with the external field perpendicular and parallel to the platelet planes. With the help of the real density matrix approach, we calculate the linear electro-optical functions of CdSe nanoplatelets, taking into account the effect of a dielectric confinement on excitonic states. The impact of platelet geometry (thickness, lateral dimension), and on the applied field strength, on the spectrum, is discussed.

Keywords: electroabsorption; nanoplatelets; CdSe; exciton states; Franz-Keldysh effect

PACS: 71.35.-y; 78.20.-e; 78.40.-q

1. Introduction

We concentrate our attention on semiconductor nanostructures, called nanoplatelets (NPL), which are quantum dots (QDs), but with different confinement mechanism, compared with other (for example GaAl/GaAlAs) QDs and quantum wells (QWs) which we call standard QDs (QWs). In the standard QDs the electrons and the holes, created by the wave propagating in a QW, are confined in a nanostructure of one type of semiconductors by an impenetrable barrier of a different semiconductor. In the considered below CdSe NPLs the confinement is of electrostatic origin and is made by a large dielectric contrast between the semiconductor (here CdSe) and its environment. Despite this difference, electrons and holes interact by a screened Coulomb potential, and bound electron-hole pairs, named excitons, are created. Colloidal group II-VI semiconductor nanostructures have emerged as one of the most studied inorganic systems. The quite uncomplicated synthesis and the ability to tune optical properties depending on their crystalline size due to the quantum confinement effect¹ make them good candidates for highly efficient light emitters, bioimaging markers, and photovoltaic cells. Colloidal nanoplatelets (NPLs) are cuboid nanostructures with the thickness of several atomic layers and much larger lateral size so that the confinement is strong only in the thinnest dimension. In the two last decades, after the first synthesis of CdSe NPLs, [1], a large number of works dedicated to this topic, appeared. A small selection of them is given in references [1]-[18].

As in standard QDs, the optical properties of NPLs are dominated by excitons. So the major part of the initial research on NPLs was concentrated on the calculation of exciton characteristics, such as exciton binding energy, confinement eigenfunctions, and eigenvalues.

Similar to the case of other nanostructures, the next development was directed at electro- and magneto-optical properties. CdSe nanoplatelets (NPLs) have unique electro-optical properties due to strong 1D quantum confinement, featuring giant oscillator strength (GOST), narrow absorption/emission, large absorption cross-sections, high exciton binding energies, and excellent optical gain, making them ideal for LEDs, lasers, and sensors, with thickness dictating color and surface chemistry (ligands/doping) tuning efficiency and spectral features like their strong Stark effect under electric fields. Beginning with the pioneering work by Miller *et. al.* [19], where the term 'Quantum Confined Stark Effect' (QCSE) was introduced, the optical response of quantum semiconductor nanostructures (wells, dots, wires) subjected to an interaction with the external constant electric field, has attracted many interest over the past decades, for example, [20]-[22]). Besides the cognitive value, this attention is motivated by possible technological applications of QCSE, for example, Self-Electrooptic Effect Devices (SEEDs), fast optical switches and modulators, crucial for optical communications (for example, [23]).

The optical properties of NPLs, including electro-absorption, were subject of extensive experimental and theoretical studies (for example, [22]). However, it seems, that there are few theoretical articles on electro-optical effects. This makes an inspiration to the present work. We will discuss the effects of applied static electric field on NPL with dielectric confinement. The electron-hole Coulomb potential dielectrically screened with the static dielectric constant is adopted, and the valence band structure is considered in the cylindrical approximation, thus separating light- and heavy hole motions. In calculations we use the so-called Real Density Matrix Approach (RDMA) (see Ref. [24] for details about RDMA). This method enables to obtain analytic expressions for the NPLs electro-optical functions, where we have chosen the electro-absorption coefficient.

The paper is organized as follows. In Sect. 2 we present the calculation method, based on RDMA. In Sections 3 and 4 we discuss the case of the electric field applied parallel to the NPL growth axis (z-axis). In the next section we analyze the case of the field applied parallel to the NPL plane, when the exciting electromagnetic wave energy is below the fundamental gap. The case with the field applied parallel to the NPL plane, when the exciting wave energy exceeds the fundamental gap, is discussed in Sect. 6. We close with conclusions in Sect. 7. Appendices A and B contain calculation details.

2. The Method

The real density matrix approach (RDMA) seems to be especially appropriate for computing the effects of external fields since it includes both the relative motion of the carriers and the center-of-mass motion, where the interaction with the radiation field takes place.

We analyze the weak field limit, where the set of basic RDMA equations ('constitutive equations') reduces to a set of linearized equations which are the inter-band equations with only the linear source on the right-hand-side retained. The resulting linearized equations for the coherent amplitudes for the electron-hole pair of coordinates $\mathbf{r}_1 = \mathbf{r}_h$ and $\mathbf{r}_2 = \mathbf{r}_e$ between any pair of bands α (valence band) and b (conduction band) read:

$$-i(\hbar\partial_t + \Gamma_{\alpha b})Y_{12}^{\alpha b} + H_{eh\alpha b}Y_{12}^{\alpha b} = \mathbf{M}_{\alpha b}\mathbf{E}, \quad (1)$$

where $\Gamma_{\alpha b} = \hbar/T_2^{\alpha b}$ is a phenomenological damping coefficient, \mathbf{E} is the electric vector of the impinging electromagnetic wave, and $\mathbf{M}_{\alpha b}$ is the inter-band transition dipole density. The notation $Y_{12}^{\alpha b} = Y^{\alpha b}(\mathbf{r}_1, \mathbf{r}_2)$ is used. When external static fields \mathbf{F} (electric field), and \mathbf{B} (magnetic field), are applied, the effective-mass two-band Hamiltonian $H_{eh\alpha b}$ with gap $E_{g\alpha b}$ for any pair of bands is

$$\begin{aligned} H_{eh\alpha,b} = & E_{g\alpha b} + \frac{1}{2m_e} \left(\mathbf{p}_e - e \frac{\mathbf{r}_e \times \mathbf{B}}{2} \right)^2 \\ & + \frac{1}{2m_h} \left(\mathbf{p}_h + e \frac{\mathbf{r}_h \times \mathbf{B}}{2} \right)^2 + e\mathbf{F} \cdot (\mathbf{r}_e - \mathbf{r}_h) \\ & + V_{\text{conf}}(\mathbf{r}_e, \mathbf{r}_h) - \frac{e^2}{4\pi\epsilon_0\epsilon_1|\mathbf{r}_e - \mathbf{r}_h|}, \end{aligned} \quad (2)$$

choosing appropriate values of E_{gab} and the effective mass tensors $\underline{m}_{e,h'}$, and V_{conf} are the surface potentials for electrons and holes. The coherent amplitudes Y_{12}^{ab} determine the total NPL polarization

$$\mathbf{P}(\mathbf{R}) = 2 \sum_{\alpha, \dots, b, \dots} \text{Re} \mathbf{M}_{c\nu}(\mathbf{r}) Y^{c\nu}(\mathbf{R}, \mathbf{r}), \quad (3)$$

where the summation includes all allowed excitonic transitions between the valence ($w = \alpha, \beta \dots$) and conduction ($c = a, b, \dots$) bands, \mathbf{R} and \mathbf{r} are the electron-hole pair center-of-mass and the relative coordinate, respectively. The equations (1)-(3) connect the polarization to the electric field. In addition, the electric field must obey the Maxwell equation

$$-c^2 \epsilon_0 \nabla \times \nabla \times \mathbf{E} - \epsilon_0 \epsilon_1 \ddot{\mathbf{E}} = \ddot{\mathbf{P}}, \quad (4)$$

where the polarization is given in Eq.(3), and ϵ_1 is the dielectric constant of the material contained inside the NPL.

The RDMA scheme, described by Eqs. (1)-(4), is solved in the following steps.

1. We solve Eq. (1), with the Hamiltonian (2), to obtain the excitonic amplitudes Y_{12}^{ab} .
2. Having calculated the amplitudes, we use them in Eq. (3) and, in the long wave approximation, determine the NPL susceptibility.
3. The so obtained susceptibility enables to calculate the optical functions (electro-reflectivity, transmissivity, absorption).

We consider dipole-allowed transitions at the Γ point of the Brillouin zone within a simple two-band model. Further, we assume that the electric field \mathbf{E} is linearly polarized with a component E_x and that the vector \mathbf{M} has a non-vanishing component $M_x(\mathbf{r})$ in the same direction. For the quantities Y, \mathbf{E} and \mathbf{P} the center-of-mass dependence is of the plane-wave form $\exp(ik_z Z - i\omega t)$. As in previous works, in the NPL internal region we separate the exciton center-of-mass and relative motion, and consider the case $\mathbf{B}, \mathbf{F} \parallel z$. This assumption forces the cylindrical symmetry, and the Hamiltonian (2) is transformed into the form

$$\begin{aligned} H = & E_g + \frac{p_{hz}^2}{2m_{hz}} + V_h(z_h) + \frac{p_{ez}^2}{2m_{ez}} + V_e(z_e) \\ & + \frac{1}{2\mu_{\parallel}} (\mathbf{p}_{e\rho}^2 + \mathbf{p}_{h\rho}^2) + V_e(\rho_e) + V_h(\rho_h) \\ & + \frac{1}{8} \mu_{\parallel} \omega_c^2 \rho^2 + \frac{e}{2\mu'_{\parallel}} B \mathcal{L}_z + eF(z_e - z_h) \\ & - \frac{e}{M_{\parallel}} \mathbf{P}_{\parallel} \cdot (\boldsymbol{\rho} \times \mathbf{B}) - \frac{e^2}{\sqrt{\rho^2 + (z_e - z_h)^2}}, \end{aligned} \quad (5)$$

where the cyclotron frequency is

$$\omega_c = \frac{eB}{\mu_{\parallel}}, \quad (6)$$

and the reduced mass μ'_{\parallel} is defined as

$$\frac{1}{\mu'_{\parallel}} = \frac{1}{m_{e\parallel}} - \frac{1}{m_{h\parallel}}. \quad (7)$$

The operator \mathcal{L}_z is the z -component of the angular-momentum operator. We must solve the constitutive equations with the above Hamiltonian to obtain the polarization and finally the optical functions. Since we aim to analyze the electro-optical effects, all terms in the Hamiltonian (5) related to the magnetic field will be put equal zero.

3. The Electric Field Parallel to the Z-Axis

We will discuss the changes of the NPL optical response when a constant external electric field \mathbf{F} is applied in the z -direction. We consider a CdSe nanoplatelet of cuboid shape, located at the $z = 0$ plane, and with the barriers located at $x = \pm L_x/2, y = \pm L_y/2, z = \pm L_z/2$. Typically, for NPLs the vertical dimension ("thickness") L_z is of the order of a few monolayers, which, for example, in the below considered CdSe NPLs, means 1-2 nm. The lateral extension is much larger, mostly several dozen nm. A schematic picture of a nanoplatelet is displayed in Figure 1.

As was merely proved, the small vertical extension forces changes in electron and hole effective masses. They increase with decreasing thickness. This situation is illustrated in Table 1. We consider the response of the NPL to a normally incident electromagnetic wave, linearly polarized in the x -direction

$$\mathbf{E}_i(z, t) = \mathbf{E}_{i0} \exp(ik_0z - i\omega t), \quad k_0 = \frac{\omega}{c}. \quad (8)$$

Table 1. Masses, reduced masses, Rydberg energies, Luttinger parameters, and coherence radii, from Ref. [14]. Lengths in nm, masses in free electron mass m_0 , energies in meV, ML means 'monolayers'.

Parameter	3ML	4ML	5ML
L_z	1	1.33	1.67
m_{ez}	0.2567	0.2015	0.1635
$m_{e\parallel}$	0.3208	0.2519	0.2044
a_{ez}^*	1.236	1.575	1.94
m_{hzH}	1.1925	0.9754	0.8153
$m_{h\parallel H}$	0.4957	0.4337	0.3879
m_{hzL}	0.4149	0.3659	0.3302
$m_{h\parallel L}$	0.8121	0.6887	0.5963
μ_{zH}	0.2112	0.167	0.1362
μ_{zL}	0.1586	0.13	0.1094
a_{ez}^*	1.236	1.575	1.94
$a_{e\parallel}^*$	0.989	1.26	1.55
a_{hzH}^*	0.266	0.325	0.389
a_{hzL}^*	0.765	0.867	0.961
E_{ez}	918.13	686.81	530
E_{hzH}	221.13	162.1	130
E_{hzL}	579.53	352.26	277.58
E_{zH}	1139.4	816.8	636
E_{zL}	1497.4	1036.5	783.1
R_{ez}^*	96.98	76.12	61.77
$R_{\parallel H}^*$	73.58	60.20	51.28
R_{hzH}^*	450.5	368.5	308
R_{hzL}^*	156.74	138.23	124.66
$R_{\parallel L}^*$	86.88	69.67	57.49
γ_1	1.6243	1.8789	2.1062
γ_2	0.3929	0.4269	0.4488
ρ_{0H}	0.20	0.18	0.17
ρ_{0L}	0.22	0.19	0.18

The movement of electrons and the holes in the z direction is affected by the dielectric confinement potential, which we take in the form

$$V_{e,h}(z) = \frac{\gamma_{e,h}}{(L/2) - z}. \quad (9)$$

The coefficient γ is proportional to dielectric permittivities [25]-[27]

$$\gamma \propto \frac{\epsilon_1 - \epsilon_2}{\epsilon_1(\epsilon_1 + \epsilon_2)}, \quad (10)$$

where $\epsilon_2(\epsilon_{out})$ and $\epsilon_1(\epsilon_{in})$ are the permittivities of surrounding environment (ligands) and internal media, respectively, and $\epsilon_2 \ll \epsilon_1$. Using the potential (9) we solve the corresponding Schrödinger equation [14]. The resulting eigenvalues, demonstrating the impact of the permittivities, are given in Appendix A, Eq. (A1). In the calculations we have used the values $\epsilon_1 = 6$, $\epsilon_2 = 2$ [5].

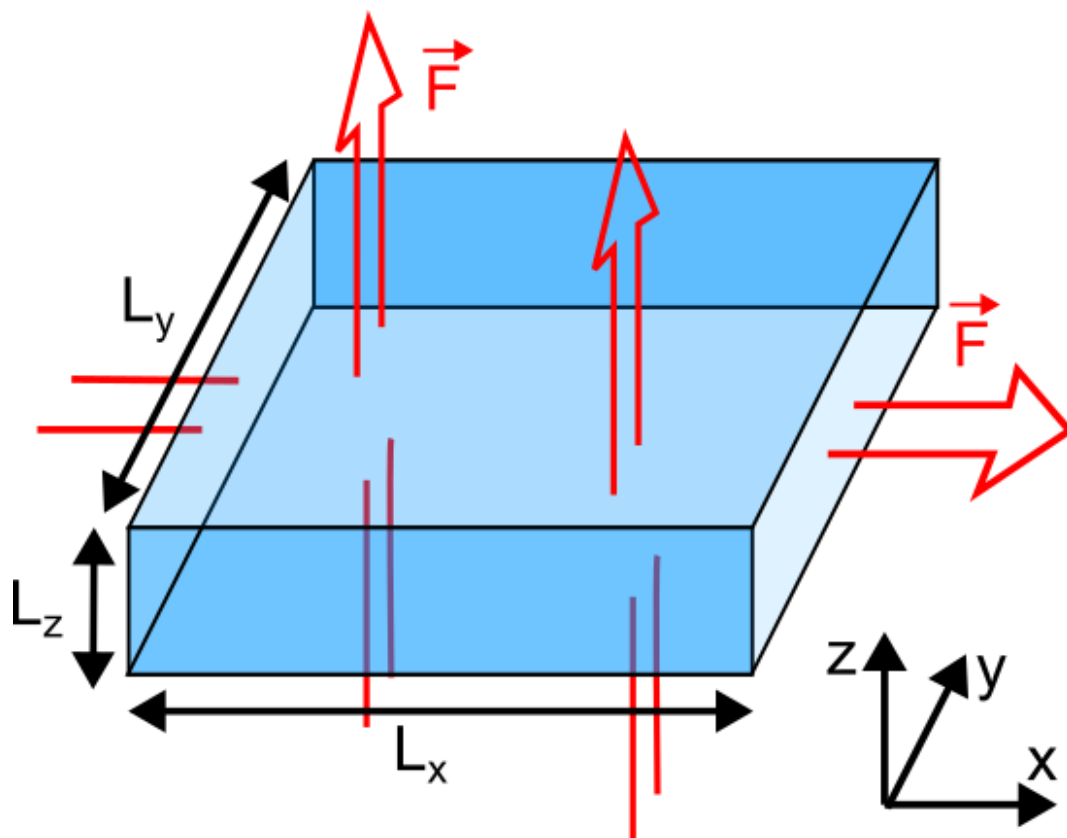


Figure 1. Schematic picture of a nanoplatelet. Two discussed applied field orientations are indicated.

The calculations of electro-optical properties become much simpler when we consider an NPL of thickness L_z , with parabolic confinement potentials in the form of an harmonic oscillator potential

$$V_{\text{conf}} = \frac{1}{2}m_{ez}\omega_{ez}^2z_e^2 + \frac{1}{2}m_{hz}\omega_{hz}^2z_h^2, \quad (11)$$

where the energies $\hbar\omega_{ez}, \hbar\omega_{hz}$ correspond to the electron and hole barriers. When concerning the in-plane electron and hole motion, we retain the assumptions presented in Ref. [14], where the cuboidal NPL is replaced by a cylinder of height L_z , and a radius $r_{eff} = \sqrt{L_x L_y / \pi}$. We neglect the motion of the hole, and the electron moves under the influence of the Coulomb attraction with the hole located at the point $\rho = 0, z = 0$, and the confinement potential

$$V_e(\rho_e) = \begin{cases} 0 & \text{for } \rho_e \leq R, \\ \infty & \text{for } \rho_e > R. \end{cases} \quad (12)$$

where we put $R = r_{eff}$. In this case, and with the applied constant electric field, the NPL Hamiltonian has the form

$$\begin{aligned} H &= E_g + H_{m_{ez}, \omega_{ez}}^{(1D)}(z_e) + H_{m_{hz}, \omega_{hz}}^{(1D)}(z_h) \\ &+ H_{Coul}^{(2D)}(\rho) + eF(z_e - z_h) \\ &+ \frac{e^2}{4\pi\epsilon_0\epsilon_b\rho_e} - \frac{e^2}{\sqrt{\rho_e^2 + (z_e - z_h)^2}}, \end{aligned} \quad (13)$$

containing the one-dimensional oscillator Hamiltonians

$$H_{m,\omega}^{(1D)}(z) = \frac{p_z^2}{2m} + \frac{1}{2}m_z\omega^2 z^2, \quad (14)$$

and the two-dimensional Coulomb Hamiltonian

$$H_{Coul}^{(2D)}(\rho) = \frac{\mathbf{p}_{\parallel}^2}{2m_{e\parallel}} - \frac{e^2}{4\pi\epsilon_0\epsilon_b\rho_e} + V_e(\rho_e). \quad (15)$$

Using the substitution

$$\zeta_e = z_e + z_{0e}, \quad z_{0e} = \frac{eF}{m_{ez}\omega_{ez}^2}, \quad (16)$$

$$\zeta_h = z_h - z_{0h}, \quad z_{0h} = \frac{eF}{m_{hz}\omega_{hz}^2}, \quad (17)$$

we obtain the QW Hamiltonians in the form

$$\begin{aligned} H &= E_g + H_{m_{ez}, \omega_{ez}}^{(1D)}(\zeta_e) + H_{m_{hz}, \omega_{hz}}^{(1D)}(\zeta_h) \\ &- \frac{(eF)^2}{2m_{ez}\omega_{ez}^2} - \frac{(eF)^2}{2m_{hz}\omega_{hz}^2} + H_{Coul}^{(2D)}(\rho_e) \\ &+ \frac{e^2}{4\pi\epsilon_0\epsilon_b\rho_e} - \frac{e^2}{\sqrt{\rho_e^2 + (z_e - z_h)^2}}. \end{aligned} \quad (18)$$

With the above QW Hamiltonians we can solve the constitutive equations

$$(H - \hbar\omega - i\Gamma)Y = \mathbf{ME}. \quad (19)$$

We use the long wave approximation, and seek solutions in the form

$$\begin{aligned} Y(\rho_e, \zeta_e, \zeta_h) &= E(Z) \sum_{jm} Y_{0,jm} \psi_{jm}(\rho_e) \\ &\times \psi_{\alpha_{ez}}^{(1D)}(\zeta_e) \psi_{\alpha_{hz}}^{(1D)}(\zeta_h), \end{aligned} \quad (20)$$

where ψ_{jm} are the eigenfunctions of the Hamiltonian (15),

$$\begin{aligned} \psi_{jm}(\xi, \phi) &= C \xi^{|m|} e^{-\xi/2} \\ &\times M\left(m + \frac{1}{2} - \eta, 2|m| + 1; \xi\right) \frac{e^{im\phi}}{\sqrt{2\pi}}. \end{aligned} \quad (21)$$

Here j and m are the principal and magnetic quantum numbers of the 2-dimensional excitonic state, $M(a, b, z)$ is the confluent hypergeometric function (notation by Ref. [28]), $\rho = \rho_e / a_{e\parallel}^*$, and we used notation

$$\begin{aligned}\eta &= \frac{2}{\kappa}, \quad \zeta = \kappa \rho, \quad a_{e\parallel}^* = \frac{m_0}{m_{e\parallel}} \epsilon_1 a_B^*, \\ \kappa^2 &= -4 \frac{2m_{e\parallel}}{\hbar^2} a_{e\parallel}^{*2} E = 4/\epsilon,\end{aligned}$$

where m_0 is the free electron mass, and $a_B^* = 0.0529$ nm the hydrogen Bohr radius. The functions $\psi_{\alpha_z, N}^{(1D)}(z)$ ($N=0,1,\dots$) are the quantum oscillator eigenfunctions of the Hamiltonian (14),

$$\begin{aligned}\psi_{\alpha_z, N}^{(1D)}(z) &= \pi^{-1/4} \sqrt{\frac{\alpha_z}{2^N N!}} H_N(\alpha_z z) e^{-\frac{\alpha_z^2}{2} z^2}, \\ \alpha_z &= \sqrt{\frac{m_z \omega_z}{\hbar}},\end{aligned}\quad (22)$$

$H_N(x)$ being Hermite polynomials ($N = 0, 1, \dots$). We consider in detail the lowest confinement state $N_e = N_h = 0$.

For further calculations we must define the dipole density \mathbf{M} . Having in mind the experiments from Refs. [22], and [6], where resonances due to 1SH and 1SL excitons were observed, we choose \mathbf{M} in the form

$$\mathbf{M}_{S,\alpha}(\mathbf{r}) = \mathbf{M}_{0,S\alpha} N_{S\alpha} \exp(-\rho/\rho_{0\alpha}) \delta(z_e - z_h), \quad (23)$$

where $\rho_{0\alpha}$ are the so-called coherence radii

$$\rho_{0H} = \sqrt{\frac{R_{\parallel H}^*}{E_g}}, \quad \rho_{0L} = \sqrt{\frac{R_{\parallel L}^*}{E_g}}, \quad (24)$$

and $N_{S,\alpha}$ are normalization constants

$$N_{S,\alpha} \int_0^{\mathcal{R}} \rho \exp(-\rho/\rho_{0\alpha}) d\rho = 1. \quad (25)$$

The integrated dipole strengths $\mathbf{M}_{0,S\alpha}$ for CdSe NPLs of various sizes, are given in Ref. [14]

Inserting the series (20) into constitutive equation (19) we calculate the expansion coefficients $Y_{0,jm}$. The so obtained exciton amplitudes are used in Eq. (3), giving the NPL polarization and, by relation $\mathbf{P} = \epsilon_0 \chi \mathbf{E}$, the susceptibility χ

$$\chi = \frac{2}{\epsilon_0} \sum \frac{|\langle M | \psi_{jm}(\rho_e) \psi_{\alpha_{ez}}^{(1D)}(\zeta_e) \psi_{\alpha_{hz}}^{(1D)}(\zeta_h) \rangle|^2}{E_{res,jm} - \hbar\omega - i\Gamma}, \quad (26)$$

where the summation runs over the excitonic transitions taken into account. The exciton resonance energies are defined by the relation

$$\begin{aligned}E_{res,jm} &= E_g + W_{0e} + W_{0h} + E_{jm} \\ &+ \left\langle \frac{2}{\rho} \right\rangle + \Delta E + E_{b,jm},\end{aligned}\quad (27)$$

where

$$W_{0e,h} = \frac{1}{2} \hbar \omega_{e,hz}, \quad (28)$$

$$\left\langle \frac{2}{\rho} \right\rangle = 2R_{e\parallel}^* \int_0^R d\rho \psi_{jm}^2(\rho), \quad (29)$$

$$\Delta E = -\frac{(eF)^2}{2m_{ez}\omega_{ez}^2} - \frac{(eF)^2}{2m_{hz}\omega_{hz}^2}, \quad (30)$$

and E_{jm} are the eigenvalues of the operator (15), ΔE is the Stark shift. The excitonic binding energy $E_{b,jm}$ is defined as

$$E_{b,jm} = -2R_{e\parallel}^* \int_{-\infty}^{\infty} \int_{-\infty}^{\infty} dz_e dz_h \left(\psi_{\alpha_{ez}}^{(1D)} \right)^2(z_e) \left(\psi_{\alpha_{hz}}^{(1D)} \right)^2(z_h) \\ \times \int_0^R \frac{\psi_{jm}^2(\rho) \rho d\rho}{\sqrt{\rho^2 + (z_e - z_h)^2}}. \quad (31)$$

4. Results of Specific Calculations for $F \parallel z$

We performed calculations for 3 CdSe nanoplatelets analyzed in Ref. [6], with sizes

- 3ML $1.0 \times 56 \times 41$ nm,,
- 4ML $1.33 \times 17 \times 15$ nm,
- 5 ML $1.67 \times 30 \times 11$ nm.

All the parameters used in the calculations are collected in Table 1. We have calculated the Stark shift, depending on the lateral dimension L_z , and the applied field strength F , obtaining the result

$$\Delta E_{H,L} = -C \left(\frac{F}{F_{IB}} \right)^2 M_{zH,L} L_z^4, \quad (32)$$

where

$$C = \frac{R_B^{*3}}{(556)^2} = 8.137 \times 10^6, \quad (33)$$

and $M_{zH,L} = m_{ez} + m_{hzH,L}$ is the total exciton mass in the z -direction. The quantity F_{IB} represents the ionization field strength

$$F_{IB} = 2.57 \times 10^6 \frac{\text{kV}}{\text{cm}}. \quad (34)$$

The details of the calculations are given in Appendix A

Using the eigenfunctions (22), and the dipole densities (23), we calculated the oscillator strengths (the part related to the vertical motion), obtaining the expression

$$f_{L_z,F} = \exp\left(-1.15 M_z L_z^2 \cdot 10^{-4} x^2\right). \quad (35)$$

The dependence on the applied field strength is depicted in Figure 2. We observe the decreasing of oscillator strengths with the increasing field strength.

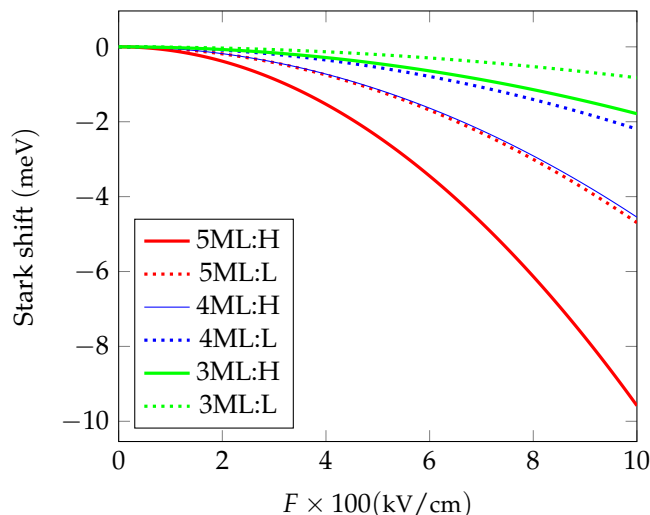


Figure 2. Stark shift for CdSe NPLs and heavy-hole excitons (solid lines), and light-hole excitons (dotted lines).

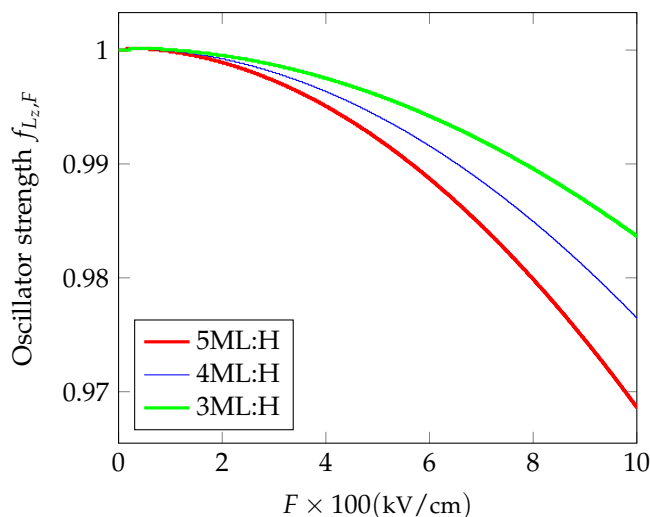


Figure 3. Oscillator strengths f_z dependence on applied field strength.

Finally, we have calculated the absorption coefficient, as the imaginary part of the susceptibility (26). In this equation the resonance energies $E_{res, jm}$ are needed. An important component of the resonance energy is the exciton binding energy, defined in Eq. (31). We observe that the binding energy decreases with the increasing field, as shown in Figure 4. In consequence, the resonance energies increase, despite of the Stark shift, acting in opposite direction. The absorption maxima are shifted versus higher energies (smaller wave lengths), in difference to the behavior in quantum wells. Such shift was observed in experiments by Baghdasaryan et al. [22]. Besides, the heavy- end light exciton absorption maxima are nearing and merge in the limit of high fields (Figure 6). The dependence of the binding and resonance energies, and the absorption coefficient, on the applied field strength, is shown in Figs. 4-6.

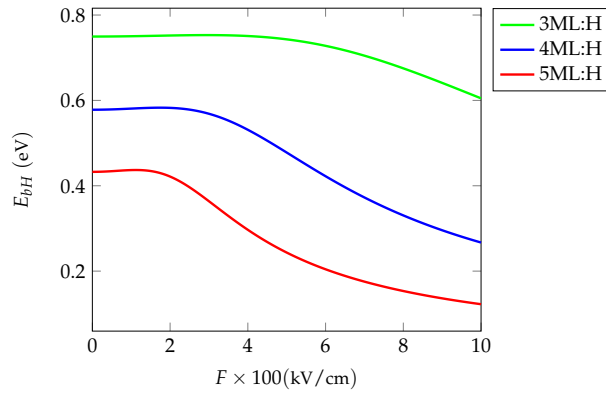


Figure 4. Exciton binding energy for heavy holes *versus* applied field strength.

Table 2. Sizes and exciton states energies, transition matrix elements M , oscillator strengths, and damping parameters, for disks analyzed by Brumberg *et al.* [6], lengths in nm, matrix elements M in $e \cdot \text{nm}$, energies in meV, the energy gap at room temperature 1750 meV, notation: 1: 56×41 , 3ML, 2: 17×15 , 4ML 3: 30×11 , 5ML, 4: 17×15 , 4ML, 5: 30×11 , 4ML, 6: 56×41 , 4ML.

lat. extension	1	2	3	4	5	6
$a_{e\parallel}^*$	1	1.26	1.553	1.26	1.26	1.26
r_{eff}	27	9	10.25	9	10.25	27
\mathcal{R}	27	7.15	6.6	7.15	8.134	21.455
1SH	2640.44	2382.2	2242.2	2540	2537.7	2531
λ	469.2	520.5	553	488.6	489	490.4
1SL	3178.4	2745.25	2498.4	2761	2758.7	2752
λ	390	451.68	496.31	449.5	449.8	450.9
M_{0SH}	0.625	0.22	0.19	0.22	0.19	0.625
f_{SH}	4.16	4.77	5.47	4.77	4.6	4.96
f_{SL}	3.72	3.75	4.77	3.75	4.44	4.41
Γ_{SH}	4.63	2.53	2.86	2.53	2.86	2.86

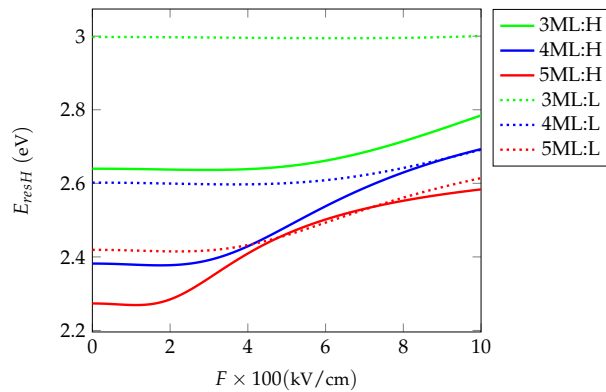


Figure 5. Resonance energies for heavy (H) and light (L) hole exciton vs applied field strength.

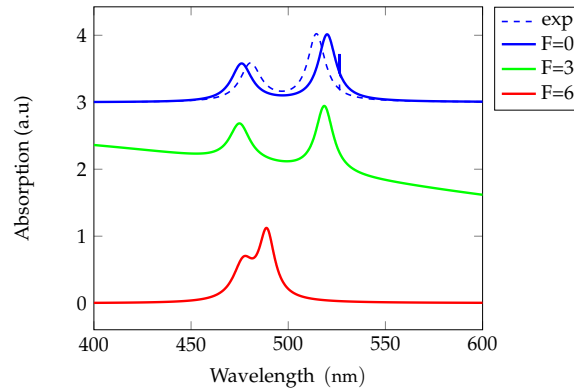


Figure 6. Normalized absorption for the case 'Thickness' at 273 K, for three values of the applied field in the case 4ML thickness. The dashed curve represents experimental data from Ref. Geiregat *et al.* [9]

5. The Electric Field Parallel to the NPL Plane, Excitation Below Gap

In this section we analyze the electro-optical effects, when the external electric field F is applied parallel to the NPL-plane, choosing the axis $0x$. The considered case is more complicated than the case $F \parallel z$, where the electric field was decoupled from the 2-dimensional Coulomb potential, acting in the $x - y$ plane. Here the field, parallel to the x -axis, acts in the same plane as the cylindrically symmetric Coulomb potential, which makes impossible to find analytic solution of the relevant Schrödinger equation. To have an insight into the effects of the electric field, we have chosen a 2-dimensional model, where the electron is moving along the x axis in the interval $-L_x/2 \leq x \leq L_x/2$, and we maintain the electron and hole movement in the z -direction, in the plane $x, y = 0$. With this assumptions the relevant Hamiltonian has the form

$$\begin{aligned}
 H &= E_g + H_{m_{ez}, \omega_{ez}}^{(1D)}(z_e) + H_{m_{hz}, \omega_{hz}}^{(1D)}(z_h) \\
 &+ V(x) + H_{\text{Coul}}^{(1D)}(x) + eFx \\
 &- H_{\text{Coul}}^{(1D)}(x) - \frac{e^2}{\sqrt{x^2 + (z_e - z_h)^2}}, \\
 H_{\text{Coul}}^{(1D)}(x) &= -\frac{\hbar^2}{2m} \frac{d^2}{dx^2} - \frac{e^2}{4\pi\epsilon_0\epsilon_b|x|} + V(x),
 \end{aligned} \tag{36}$$

where

$$V(x) = \begin{cases} 0 & \text{for } |x| \leq L_x/2, \\ \infty & \text{for } |x| > L_x/2. \end{cases} \tag{37}$$

The eigenfunctions of the operator $H_{\text{Coul}}^{(1D)}(x)$ have the form

$$\begin{aligned}
 \psi(\xi) &= |\xi| e^{-|\xi|/2} M(1 - \eta; 2; |\xi|), \\
 \xi &= \kappa \frac{x}{a_{e\parallel}^*}, \quad \kappa = 2\sqrt{-\epsilon} = \frac{2}{\eta},
 \end{aligned} \tag{38}$$

see Appendix B. Repeating the method used in the case $F \parallel z$, i.e. replacing the eigenfunction (38) by the function (22), with appropriate values for the coefficient α , we obtain the Stark shift in the form

$$\Delta E = 4.5 \times 10^{-4} F^2, \tag{39}$$

where the results is given in meV. The magnitude of ΔE depends, besides of the field strengths F , on the NPL size, represented here by $L_x/2 = R$, see Eq. (12). The values of ΔE , for NPLs with different sizes, are displayed in Figure 7. It should be noted, that the presented values are larger, in order of magnitude, than the Stark shift for the field applied in the z -direction (Figure 1). The

curves representing the Stark shift in Figure 7 should begin at the point $F = 0$. However, they are very close, therefore, for a better presentation, they are spread out by a small amount. Interestingly, that despite of the large simplification, the obtained eigenvalues are in a good agreement with the experimental values for $F = 0$ presented in Ref. [6], see Figure 8. Using the data presented in Tab. 3 we have calculated the normalized absorption, which shows the dependence on the NPL size, and on the applied field strength.

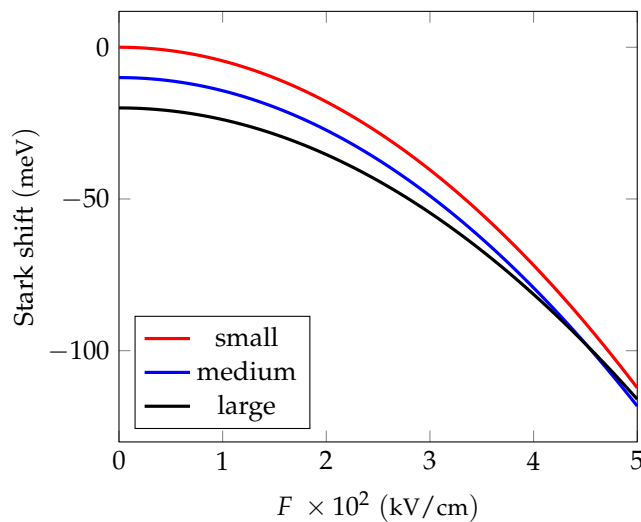


Figure 7. Stark shift for CdSe NPLs and heavy-hole excitons, for $F \parallel x$

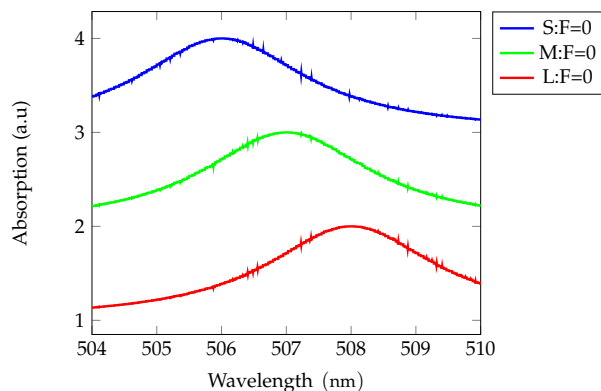


Figure 8. The shift in the heavy-hole exciton energy as the lateral size of the NPL increases, for $F = 0$.

Table 3. Parameters for calculating the Stark shift, excitonic resonance energies vs applied field strength and lateral area, field strength in kV/cm, $X = 10^2 F$, energies in meV, wavelengths in nm, oscillator strength to be multiplied by 10^{-3} .

Param.	17×15	30×11	56×41
α^{-2}	3.283	3.22	3.03
α^{-4}	10.78	10.375	9.22
$10^5 \cdot \zeta_0 / F^2$	1.89	1.82	1.62
$10^6 \cdot \Delta\varepsilon / F^2$	4.72	4.55	4.04
$10^4 \Delta E / F^2$	4.5	4.33	3.85
	$X = 0$		
$ E_b $	227.9	226.38	281.76
E_{resH}	2450.166	2448	2441
λ	506	506.54	508
E_{resL}	2670.166	2668	2661
λ	464.39	464.77	466
	$X = 0.5$		
$ E_b $	243.52	243.04	241.67
E_{resH}	2408.3	2410.5	2417.36
λ	514.88	514.41	512.95
E_{resL}	2628.3	2630.5	2637.6
λ	471.8	471.4	470.12
	$X = 1$		
$ E_b $	288.15	287.46	278.72
E_{resH}	2360.2	2362.84	2377.42
λ	525.36	524.79	521.57
E_{resL}	2580	2582.84	2597.42
λ	480.6	480.1	477.4
	$X = 2$		
$ E_b $	478.49	481.63	477.2
E_{resH}	2174.45	2173	2177.42
λ	570.25	570.63	569.48
E_{resL}	2394.45	2393.0	2397.4
λ	517.86	518.18	517.22

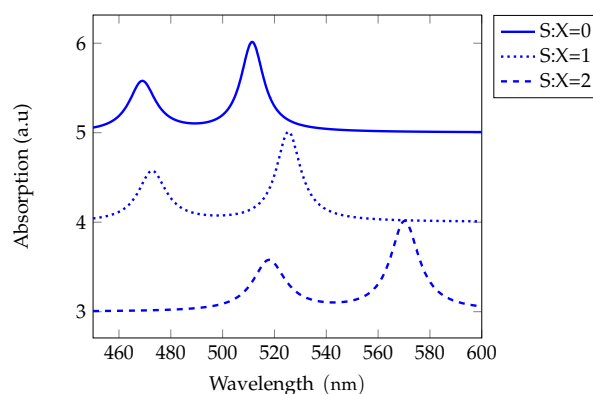


Figure 9. Normalized absorption for the case 'Lateral Area' at 273 K, for three values of the applied field in the case 4ML thickness and area 17×15 (S ="small"), field strength in $10^2 \times$ kV/cm.

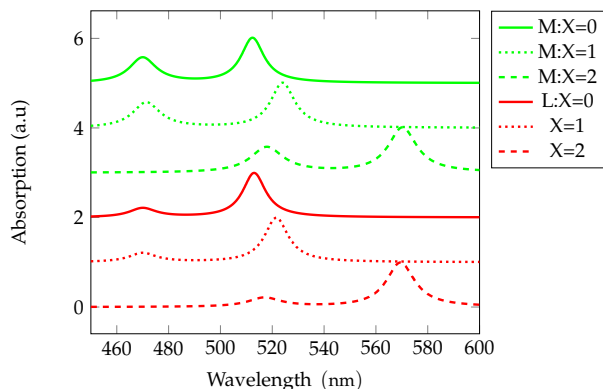


Figure 10. Normalized absorption for the case 'Lateral Area' at 273 K, for three values of the applied field in the case 4ML thickness and area 30×11 (M ="medium"), 51×41 (L ="large"), field strength in $10^2 \times \text{kV/cm}$.

6. Quantum Confined Franz-Keldysh Effect

When the excitation energy exceeds the total confinement energy (including the energy gap), and an external electric field is applied parallel to the NPL plane, oscillations in the optical functions appear which, in the case of unbounded media, are known as the Franz-Keldysh effect (see, for example, [29]). For the unbounded media they have the form of outgoing waves, with variable periodicity and amplitudes (see, for example, [30,31]). The situation changes, when the medium, as considered here NPL, is finite. Instead of outgoing waves, standing waves appear, with periodicity and amplitude depending both on the applied field strength, and on the NPL size. This effect can be called Quantum Confined Franz-Keldysh effect (QCFKE). Such term appeared previously [32], but in the cited paper only a partial confinement was considered (QW), the field was applied in the z -direction, and the effect appears in the limits $L_z \rightarrow \infty$. The situation considered below is quite different, the confinement is applied in 3 direction, and the term Quantum Confined Franz-Keldysh effect seems to be justified. In the considered excitation region one can, in lowest approximation, neglect the e-h Coulomb interaction. Then the remaining terms in the Hamiltonian correspond to kinetic energies, and compose the total confinement. Therefore, to analyze the NPL's QCFKE, we use the constitutive equation in the form

$$\left(k^2 - \frac{d^2}{d\xi^2} + f\xi\right)Y(\xi) = \frac{1}{a_{e\parallel}^*}M(\xi)E,$$

$$k^2 = \frac{E_{conf,tot} - \hbar\omega}{R_{e\parallel}^*}, \quad (40)$$

where

$$\xi = \frac{x_e}{a_{e\parallel}^*}, \quad f = \frac{F}{F_I}, \quad F_I = \frac{R_{e\parallel}^*}{e \cdot a_{e\parallel}^*}. \quad (41)$$

In the above equations the electric field F is parallel to the x -axis, and we retained the assumptions about the hole located in the NPL center. As in the case of unbounded media, the equation (40) can be solved by using appropriate Green's function, which has the form

$$\begin{aligned}
 G(\zeta, \zeta') &= g^< \cdot g^>, \\
 g^< &= \frac{\pi}{f^{1/3}} \left\{ \text{Bi} \left[f^{1/3} \left(\zeta^< + \frac{k^2}{f} \right) \right] \right. \\
 &\quad \times \text{Ai} \left[f^{1/3} \left(\frac{k^2}{f} \right) \right] \\
 &\quad \left. - \text{Bi} \left[f^{1/3} \left(\frac{k^2}{f} \right) \right] \text{Ai} \left[f^{1/3} \left(\zeta^< + \frac{k^2}{f} \right) \right] \right\}, \\
 g^> &= \text{Bi} \left[f^{1/3} \left(\zeta^> + \frac{k^2}{f} \right) \right] \\
 &\quad \times \text{Ai} \left[f^{1/3} \left(\mathcal{L} + \frac{k^2}{f} \right) \right] \\
 &\quad - \text{Bi} \left[f^{1/3} \left(\mathcal{L} + \frac{k^2}{f} \right) \right] \text{Ai} \left[f^{1/3} \left(\zeta^> + \frac{k^2}{f} \right) \right].
 \end{aligned} \tag{42}$$

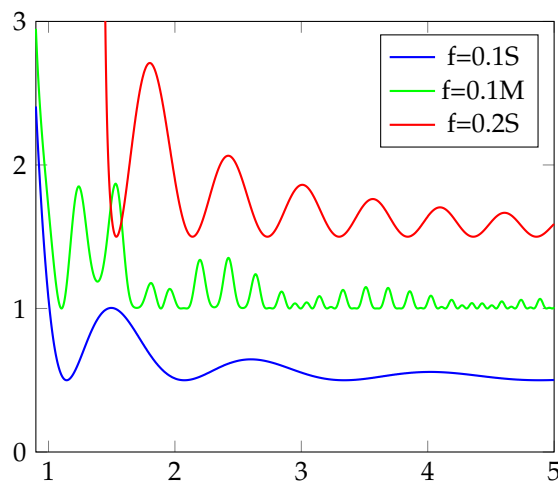
Here $\text{Ai}(z), \text{Bi}(z)$ are the Airy functions ([28]), and the notation $\zeta^<, \zeta^>$ means $\zeta^< = \min(\zeta, \zeta'), \zeta^> = \max(\zeta, \zeta')$, and $\mathcal{L} = L_x/2a_{e\parallel}^*$. The confinement effect is included since

$$G(0, \zeta') = G(\zeta, \mathcal{L}) = 0. \tag{43}$$

When the dipole density $M(\zeta)$ is defined, we obtain the NPL susceptibility in the form

$$\chi = MGM = \int_0^{\mathcal{L}} d\zeta d\zeta' G(\zeta, \zeta') M(\zeta) M(\zeta'). \tag{44}$$

The absorption coefficient is proportional to the imaginary part of the susceptibility. Its shape, showing Franz-Keldysh oscillations, is presented in Figure 11, for two values of the applied fields, and two lateral NPL dimensions. We notice the large dependence on the NPL both on the field strength, and on the size.



Energy in units of electron Rydberg above the total confinement energy

Figure 11. Absorption, $f = 0.1, 0.2, \mathcal{L} = 7.15(S), 8.134(M)$.

7. Conclusions

In this paper we have studied the electro-optical properties of CdSe NPLs with excitons, for various orientations of the applied static electric field. These properties, compared with analogous for bulk materials and QWs, show strong modifications, which are due to the total confinement of electrons and holes, with a resulting dependence of the spectra on NPLs sizes. Besides of various orientations, we have separately analyzed the two possibilities of the exciting wave energy, below and above the gap. For the energy below the gap and for both orientations of the field, we observe exciton resonances, shifted red (electric field parallel to the NPL plane), and shifted blue (electric field parallel to the z -axis). The latter effect is due to the lowering of the exciton binding energy, which prevails over the, also observed, quadratic Stark shift. In the case of the excitation energy exceeding the gap (enlarged by the confinement energy), we observe the Franz-Keldysh oscillations, with periodicity depending both on the applied field strength, and NPLs sizes. Thus, we have demonstrated that CdSe NPLs have an additional mechanism to control the exciton states not only by their thickness (z -direction) and lateral size variation, but also by the strength and orientation of an applied constant electric field. It paves the way for construction of high sensitivity modulators, based on NPLs. The obtained results agree well with the available experimental results.

Funding: The authors have no funding to declare.

Data Availability Statement: The original contributions presented in this study are included in the article/supplementary material. Further inquiries can be directed to the corresponding author.

Conflicts of Interest: The authors declare no conflicts of interest and have no competing interests.

Appendix A. Calculations of Stark Shift and Oscillator Strengths for $F \parallel z$

For calculations of the Stark shift we have to specify the confinement parameters $\alpha_{e,hz}$. They are related to the eigenvalues, which we identify with the eigenenergies for the vertical motion obtained in the case of dielectric confinement, and having the form

$$E_{e,hz} = \frac{6\beta[1 + (\gamma_{e,h}\ell_{e,h}/2)]}{m_{e,hz}L_z^2}, \quad (\text{A1})$$

which give the confinement energy

$$\begin{aligned} E_{conf} &= E_{ez} + E_{hz} \\ &= \frac{1}{\mu_z} \frac{6\beta}{L^2} + \frac{3\beta\gamma_e \ell_e}{m_{ez}L^2} + \frac{3\beta\gamma_h \ell_h}{m_{hz}L^2}, \end{aligned} \quad (\text{A2})$$

with β

$$\beta = a_B^{*2} \times R_B^* = 38 \text{ nm}^2 \text{ meV}, \quad (\text{A3})$$

where $[L] = \text{nm}$, and R_B^*, a_B^* are the hydrogen Bohr energy and hydrogen Bohr radius, respectively. Using the value of β , and the definitions

$$\ell_{e,h} = \frac{L}{2a_{ze,h}^*}, \quad a_{ze,h}^* = \frac{1}{m_{ze,h}} \epsilon_b a_B^*,$$

we obtain the confinement energy

$$\begin{aligned} E_{conf,Lv} &= \frac{1}{\mu_{zv}L^2} 228[\text{nm}^2 \text{ meV}] \\ &+ \frac{\gamma}{L} 359[\text{nm meV}], \quad v = H, L, \end{aligned} \quad (\text{A4})$$

where

$$\gamma = \gamma_e + \gamma_h, \quad v = H, L \quad (\text{A5})$$

with E given in meV and L in nm. By the relation

$$\begin{aligned} \frac{1}{\alpha_{e,hz}^2} &= \frac{\hbar}{m_{e,hz}\omega_{e,hz}} \\ &= \frac{\hbar^2}{2m_{e,hz}E_{e,hz}} = \frac{a_{e,hz}^{*2} R_{e,hz}^*}{E_{e,hz}}, \end{aligned} \quad (\text{A6})$$

one obtains

$$\alpha_{e,hz} = \frac{1}{a_{e,hz}^*} \sqrt{\frac{E_{e,hz}}{R_{e,hz}^*}}. \quad (\text{A7})$$

The quantities z_{0e}, z_{0h} are obtained by the relations

$$\begin{aligned} z_{0e,h} &= \frac{eF}{m_0 m_{e,hz} \omega_{e,hz}^2} \\ &= 2 \left(\frac{F}{F_{IB}} \right) \frac{R_B^{*2} a_B^*}{m_{e,hz} (\hbar \omega_{ez})^2}, \\ \frac{1}{F_{IB}} &= \frac{e a_B^*}{R_B^*} = 3.89 \times 10^{-7} \frac{\text{cm}}{\text{kV}}, \\ F_{IB} &= 2.57 \times 10^6 \frac{\text{kV}}{\text{cm}}. \end{aligned}$$

In the above calculations we have taken into account that the electron and hole effective masses given in Table 1 are in units of the free electron mass m_0 . Making use of the obtained expressions we arrive at the Stark shift

$$\Delta E = -\frac{(eF)^2}{2m_0 m_{ez} \omega_{ez}^2} - \frac{(eF)^2}{2m_0 m_{hz} \omega_{hz}^2}, \quad (\text{A8})$$

where

$$\frac{(eF)^2}{2m_0 m_{e,hz} \omega_{e,hz}^2} = R_B^{*3} \left(\frac{F}{F_{IB}} \right)^2 \frac{1}{m_{e,hz} (\hbar \omega_{e,hz})^2}.$$

With regard to definitions (A1) and

$$\hbar \omega_{e,hz} = 2 E_{e,hz} = \frac{556}{m_{e,hz} L_z^2} \quad (\text{A9})$$

we arrive at the Stark shift for heavy-hole and light-hole excitons in the form

$$\Delta E_{H,L} = -C \left(\frac{F}{F_{IB}} \right)^2 M_{zH,L} L_z^4, \quad (\text{A10})$$

where

$$C = \frac{R_B^{*3}}{(556)^2} = 8.137 \times 10^6, \quad (\text{A11})$$

and $M_{zH,L} = m_{ez} + m_{hzH,L}$ is the total exciton mass in the z -direction.

The oscillator strength is defined in terms of the function

$$\langle \Psi_{00} \rangle_\infty = \sqrt{\frac{\alpha_{ez} \alpha_{hz}}{p}} \exp \left[-\frac{\alpha_{ez}^2 \alpha_{hz}^2 (z_{0e} + z_{0h})^2}{2(\alpha_{ez}^2 + \alpha_{hz}^2)} \right],$$

which gives

$$f_{L_z, F} = |\langle \Psi_{00} \rangle_\infty|^2 = \frac{\alpha_e \alpha_h}{p} \\ \times \exp \left[-\frac{\alpha_{ez}^2 \alpha_{hz}^2 (z_{0e} + z_{0h})^2}{\alpha_{ez}^2 + \alpha_{hz}^2} \right], \\ p = \frac{1}{2} (\alpha_{ez}^2 + \alpha_{hz}^2),$$

Using the expressions for $\alpha_{e,hz}$ we arrive at

$$\frac{(\alpha_{ez} \alpha_{hz})^2}{\alpha_{ez}^2 + \alpha_{hz}^2} (z_{0e}^2 + z_{0h}^2) \\ = 4 \frac{6}{L_z^2} \left(\frac{F}{F_{IB}} \right)^2 M_z \frac{R_B^{*2} a_B^* L_z^4}{556^2} \\ = 760 \left(\frac{F}{F_{IB}} \right)^2 M_z = 1.15 M_z L_z^2 \cdot 10^{-4} x^2, \\ x = 10^3 F.$$

The final expression for the oscillator strength $f_{L_z, F}$ reads

$$f_{L_z, F} = \exp \left(-1.15 M_z L_z^2 \cdot 10^{-4} x^2 \right). \quad (\text{A12})$$

Appendix B. Calculations of Stark Shift and Oscillator Strengths for F in NPL Plane

In the case of applied field parallel to the NPL plane, discussed in Sec. 5, one has to solve the 1-dimensional Schrödinger equation

$$\left[-\frac{\hbar^2}{2m} \frac{d^2}{dx^2} - \frac{e^2}{4\pi\epsilon_0\epsilon_b|x|} + V(x) \right] \psi = E\psi, \quad (\text{A13})$$

with the confinement potential V defined in Eq. (37). Using scaled variables

$$\varepsilon = \frac{E}{R^*}, \quad -\frac{L_x}{2a_{e\parallel}^*} \leq x \leq \frac{L_x}{2a_{e\parallel}^*}, \\ \zeta = \kappa \frac{x}{a_{e\parallel}^*}, \quad \kappa = 2\sqrt{-\varepsilon} = \frac{2}{\eta},$$

we obtain equation

$$\frac{d^2\psi}{d\zeta^2} + \left(-\frac{1}{4} + \frac{\lambda}{\zeta} \right) \psi = 0. \quad (\text{A14})$$

It has the form of the Whittaker equation (see Ref. [28])

$$\frac{d^2W}{dz^2} + \left(-\frac{1}{4} + \frac{\eta}{z} + \frac{(1/4) - \mu^2}{z^2} \right) W = 0, \quad (\text{A15})$$

with 2 linearly independent solutions $\mathcal{M}_{\eta, \mu}(z)$, $\mathcal{W}_{\eta, \mu}(z)$, from which we choose the function $\mathcal{M}_{\eta, \mu}(z)$ finite at $z = 0$. It is related to the confluent hypergeometric function by the relation

$$\mathcal{M}_{\eta, \mu}(z) = z^{\mu+1/2} e^{-z/2} M \left(\mu - \eta + \frac{1}{2}; 2\mu + 1; z \right). \quad (\text{A16})$$

The Eq. (A14) is a special case of Eq. (A15) for $\mu = 1/2$, thus the solution of (A14) reads

$$\psi(\xi) = |\xi| e^{-|\xi|/2} M(1 - \eta; 2; |\xi|). \quad (\text{A17})$$

The eigenvalues will be obtained from the equation

$$\psi(\mathcal{L}) = 0, \quad \mathcal{L} = \frac{L_x}{2a_{e\parallel}^*}. \quad (\text{A18})$$

Using the expansion of $M(a; b; z)$ and retaining the terms at most quadratic in \mathcal{L} , we obtain the equation for eigenvalues

$$\frac{2t^2}{3} + (1 - \mathcal{L})t + 1 - \mathcal{L} + \frac{1}{3}\mathcal{L}^2 = 0, \quad (\text{A19})$$

with $t = \mathcal{L}/\eta$, and the solutions

$$\begin{aligned} t_{1,2} &= \frac{3}{4}(\mathcal{L} - 1 \pm \sqrt{\Delta}), \\ \Delta &= (1 - \mathcal{L})^2 - \frac{8}{3}\left(1 - \mathcal{L} + \frac{1}{3}\mathcal{L}^2\right) \\ &= \frac{1}{9}\mathcal{L}^2 + \frac{2}{3}\mathcal{L} - \frac{5}{3}. \end{aligned} \quad (\text{A20})$$

The equation $\Delta = 0$ defines the critical size $\mathcal{L}_{cr} = 1.93$, which means that positive solutions exist for $\mathcal{L} \geq \mathcal{L}_{cr}$. The above considered NPLs satisfy this condition.

Having calculated t , we obtain the eigenvalues by the equation

$$E = \frac{1}{\eta^2} = -\frac{t^2}{\mathcal{L}^2} R_{e\parallel}^*. \quad (\text{A21})$$

The quantity t also determines the eigenfunctions, having the form

$$\begin{aligned} \psi(u) &= 2tC\mathcal{L}u e^{-tu} \\ &\times \left[1 + (t - \mathcal{L})u + \left(\frac{2}{3}t^2 - t\mathcal{L} + \frac{1}{3}\mathcal{L}^2 \right) u^2 \right], \\ u &= \frac{\xi}{\mathcal{L}}, \end{aligned} \quad (\text{A22})$$

where C is the normalization constant.

References

1. Joo, J.; Son, J.S.; Kwon, S.G.; Yu, J.H.; and Hyeon, T. Low-temperature solution-phase synthesis of quantum well structured CdSe nanoribbons. *J. Am. Chem. Soc.* 2006, 128, 5632.
2. Achtstein, A.W.; Schliwa, A.; Prudnikau, A.; Hardzei, M.; Artemyev, M.V.; Thomsen, C.; and Woggon, U. Electronic Structure and Exciton-Phonon Interaction in Two-Dimensional Colloidal CdSe Nanosheets. *Nano Lett.* 2012, 3151-7. doi: 10.1021/nl301071n. Epub 2012 May 29.
3. Benchamekh, R.; Gippius, N.A.; Even, J.; Nestoklon, M.O.; Jancu, J.M.; Ithurria, S.; Dubertret, B.; Efros, A.L.; and Voisin, P. Tight-binding calculations of image-charge effects in colloidal nanoscale platelets of CdSe. *Phys. Rev. B* 2014, 89, 035307. DOI: <https://doi.org/10.1103/PhysRevB.89.035307>.
4. Zelewski, S.J.; Nawrot, K.C.; Źak, A.; Gładysiewicz, M.; Nyk, M.; and Kudrawiec, R. Exciton Binding Energy of Two-Dimensional Highly Luminescent Colloidal Nanostructures Determined from Combined Optical and Photoacoustic Spectroscopies. *J. Phys. Chem. Lett.* 2019, 10, 3459. doi: 10.1021/acs.jpcclett.9b00591.
5. Shornikova, E.V.; Yakovlev, D.R.; Gippius, N.A.; Qiang, G.; Dubertret, B.; Khan, A.H.; Di Giacomo, A.; Moreells, I.; and Bayer, M. Exciton binding energy in CdSe nanoplatelets measured by one- and two-photon absorption. *Nano Lett.* 2021, 21, 10525. <https://doi.org/10.1021/acs.nanolett.1c04159>.

6. Brumberg, A.; Harvey, S.M.; Philbin, J.P.; Diroll, T.; Lee, B.; Crooker, S.A.; Wasielewski, M.R.; Rabani, E.; and Schaller, R.D. Determination of the In-Plane Exciton Radius in 2D CdSe Nanoplatelets via Magneto-optical Spectroscopy, *ACS Nano* 2019, 13, 8589. <https://doi.org/10.1021/acsnano.9b02008>.
7. Yu, J.; and Chen, R. Optical properties and applications of two-dimensional CdSe nanoplatelets. *InfoMat* 2020, 2, 905. DOI: 10.1002/inf2.12106.
8. Dutta A.; Medda, A.; and Patra, A. Recent Advances and Perspectives on Colloidal Semiconductor Nanoplatelets for Optoelectronic Applications. *The Journal of Physical Chemistry C* 2021, 125, 20. <https://doi.org/10.1021/acs.jpcc.0c09416>.
9. Geiregat, P.; Rodá, C.; Tanghe, I.; Singh, S.; Alessio Di Di Giacomo, A.; Lebrun, D.; Grimaldi, G.; Maes, J.; Van Thourhout, D.; Moreels, I.; Houtepen, A.J.; and Hens, Z. Localization-limited exciton oscillator strength in colloidal CdSe nanoplatelets revealed by the optically induced stark effect. *Light: Science & Applications* 2021, 10, 112. <https://doi.org/10.1038/s41377-021-00548-z>
10. Gonçalves, I.M.; Medda, A.; Bautista, J.E.Q.; Campos, C.L.A.V.; Ghosh, S.; Patra, A.; and Gomes, S.L.A. Saturable absorption and third-order nonlinear refraction of 2D CdSe nanoplatelets resonant with heavy-hole excitonic transitions. *Appl. Phys. Lett.* 2023, 123, 251108. <https://doi.org/10.1063/5.0178578>.
11. Akhmetova, A.; Kainarbay, A.; Daurenbekov, D.; Nurakhmetov, T.; Zhangylyssov, K.; and Yussupbekova, B. Effect of Nanoplatelets Thickness on Photoluminescent, Optical, and Electronic Properties of Synthesized CdTe Semiconductor Nanoplatelets. *Crystals* 2023, 13, 1450. <https://doi.org/10.3390/cryst13101450>.
12. Koshkinbayev, Y.; Ospanova, A.; Akhmetova, A.; Nurakhmetov, T.; Kainarbay, A.; Zhangylyssov, K.; Dorofeev, S.; Vinokurov, A.; Bubenov, S.; and Daurenbekov, D. The Influence of Temperature and Stoichiometry on the Optical Properties of CdSe *Nanomaterials* 2024, 14(22), 1794; <https://doi.org/10.3390/nano14221794>.
13. Ngo, H.T. Optical and electronic properties of colloidal CdSe nanoplatelets and related heterostructures. Micro and nanotechnologies/Microelectronics. Université de Lille; Universiteit Gent 2024. ffNNT : 2024ULILN025.
14. Czajkowski, G. Optical properties of excitons in CdSe nanoplatelets. *J. Biomed. Res. Environ. Sci.* 2026 Jan 08;7(1):19. Doi: 10.37871/jbres2230, also: *arxiv* 2025. arxiv.org/pdf/2511.02857.
15. Silva, C.R. da.; Bechstedt, F.; Teles, L.K.; and Marques, M. Electronic and Optical Properties of highly Complex Ga₂O₃ Polymorphs using approximate quasiparticle DFT+A+1/2. 2024. <https://doi.org/10.1021/acs.nanolett.1c04159>.
16. Grillo, S.; Cignarella, Ch.; Bechstedt, F.; Gori, P.; Palumbo, M.; Campi, D.; Marzari, N.; and Pulci, O. Quasiparticle Effects and Strong Excitonic Features in Exfoliable 1D Semiconducting Materials, *ACS Nano* 2026, 20, 2664. <https://doi.org/10.1021/acsnano.5c14061>
17. Capellini, G.; Furthmüller, J.; Bechstedt, F.; and Botti, S. Electronic and Optical Properties of Alkaline Earth Metal Fluoride Crystals with the Inclusion of Many-Body Effects: A Comparative Study on Rutile MgF₂ and Cubic SrF₂, 2023. *Symmetry*, 15,539. <https://doi.org/10.3390/sym15020539>.
18. Furthmüller, J.; Bechstedt, F.; Botti, S.; and Cappellini, G. Influence of spin-orbit interaction and self-consistency on quasiparticle electronic structure and exciton optical spectra beyond Tamm-Dancoff: The case of BaF₂ and SrF₂. *Physical Review B* 2025. 112, 195112. DOI: <https://doi.org/10.1103/9k9g-2237>.
19. Miller, D.A.B.; Chemla, D.S.; Damen, T.C.; Gossard, A.C.; Wiegmann, W.; Wood, T.H.; and Burrus, C.A. Band-Edge Electroabsorption in Quantum Well Structures: The Quantum-Confined Stark Effect. *Phys. Rev. Lett.* 1984, 53, 2173.
20. Achtstein, A.W.; Prudnikau, A.V.; Ermolenko, M.; Gurinovich, L.I.; Gaponenko, S.V.; Woggon, U.; Baranov, A.V.; Leonov, M.Yu.; Rukhlenko, I.D.; Fedorov, A.V.; and Artemyev, M.V. Electroabsorption by 0D, 1D, and 2D Nanocrystals: A Comparative Study of CdSe Colloidal Quantum Dots, Nanorods, and Nanoplatelets. *ACS Nano* 2014. DOI: 101021/nn503745u.
21. Ziemkiewicz, D.; Czajkowski, G.; Karpiński, K.; and Zielińska-Raczyńska, S. Electro-optical properties of excitons in Cu₂O quantum wells. I. Discrete states. *Phys. Rev. B* 2021, 104, 075303. DOI: 10.1103/PhysRevB.104.075303
22. Baghdasaryan, D.A.; Harutyunyan, V.A.; and Sarkisyan, H.A. Linear and non-linear electrooptical transitions in CdSe nanoplatelets. *Optical and Quantum Electronics* 2024, 56,1221. <https://doi.org/10.1007/s11082-024-07180-2>.
23. Rong, Y.; Huo, Y.; Fei, E.T.; Fiorentino, M.; Tan, M.R.T.; Ochalski, T.; Huyet, G.; Thylen, L.; Chacinski, M.; Kamins, T.I.; and Harries, J.S. High speed optical modulation in Ge quantum wells using quantum confined stark effect. *Front. Optoelectron.* 2012, 5,82. doi.org/10.1007/s12200-012-0194-9.

24. Ziemkiewicz D.; Knez D.; Garcia, E.P.; Zielińska-Raczyńska, S.; Czajkowski, G.; Salandrino A.; Kharintsev, S.S.; Noskov, A.I.; Potma, E.O.; and Fishman, D.A. Two-Photon Absorption in Silicon Using Real Density Matrix Approach. *Journ. Chem. Phys.* 2024; 161: 144117. doi: 10.1063/5.0219329.
25. Landau, L.D.; and Lifshitz, E.M. *Electrodynamics of Continuous Media*, 2nd Ed. by E. M. Lifshitz and L. P. Pitaevskii. 1984, Pergamon Press, Oxford. ISBN 0-08-030276-9.
26. Caicedo-Davila, S.; Caprioglio, P.; Lehmann, F.; Levcenko, S.; Stolterfoht, M.; Neher, D.; Kronik, L.; and Abou-Ras, D. Effects of Quantum and Dielectric Confinement on the Emission of Cs-Pb-Br Composites, *Adv. Func. Mater.* 2023,33, 2305240. <https://doi.org/10.1002/adfm.202305240>.
27. Kurtina, D.A.; Long, H.; Chang, S.; Vasiliev, R.B. Solvent effect on chiroptical properties of chiral atomically thin CdSe nanoplatelets capped with enantiomeric ligands. *Optical Mat.* 2025, 158, 116483. <https://doi.org/10.1016/j.optmat.2024.116483>.
28. Abramowitz, M., and Stegun, I., eds. *Handbook of Mathematical Functions*. 1964, Dover Publications, ISBN 0-486-61272-4. New York, US. <http://www.ams.org/notices/201107/rtx110700905p.pdf>,
29. Kalt, H.; and Klingshirn, C.F. *Semiconductor optics*. 2019, Springer Nature, Cham, Switzerland. <https://doi.org/10.1007/978-3-030-24152-0>.
30. Zielińska-Raczyńska, S.; Ziemkiewicz, D.; and Czajkowski, G. Electro-optical properties of Cu₂O for P excitons in the regime of Franz-Keldysh oscillations. *Phys. Rev. B* 2018, 97, 165205. DOI: 10.1103/PhysRevB.97.165205.
31. Ziemkiewicz, D.; Czajkowski, G.; Karpiński, K.; and Zielińska-Raczyńska, S. Electro-optical properties of excitons in Cu₂O quantum wells. II. Continuum states II. *Phys. Rev. B* 2021, 104, 075304. DOI: 10.1103/PhysRevB.104.075304.
32. Miller, D.A.B.; Chemla, D.S.; and Schmitt-Rink, S. Relation between electroabsorption in bulk semiconductors and in quantum wells: The quantum-confined Franz-Keldysh effect. *Phys. Rev. B* 1986, 33, 6976. DOI: <https://doi.org/10.1103/PhysRevB.33.6976>

Disclaimer/Publisher's Note: The statements, opinions and data contained in all publications are solely those of the individual author(s) and contributor(s) and not of MDPI and/or the editor(s). MDPI and/or the editor(s) disclaim responsibility for any injury to people or property resulting from any ideas, methods, instructions or products referred to in the content.